J-Researchers

JOURNAL OF CIVIL ENGINEERING RESEARCHERS

Assessment of Composite Bars and FRP Panels for Seismic Bridge Decks

Amir Mohammad Bakhtiari,[a,*] Ali Harati[a]

[a]*Department of Civil Engineering, Arman Institution of Engineering and Technology, Tehran, Iran*

Journals-Researchers use only: Received date: 2023.06.21; revised date: 2023.08.10; accepted date: 2023.09.19

Abstract

Seismic Strengthening offers a cost-effective and sustainable solution for constructing bridges in seismic zones. In these rehabilitation interventions, Fiber Reinforced Polymer (FRP) composites are often used instead of steel members due to their lightweight nature, high strength, and excellent corrosion resistance. Researchers are now focusing on creating innovative FRP-concrete hybrid structures. This study specifically investigates the numerical modeling of the response of a hybrid FRP-concrete jacket bridge pier subjected to quasi-static tests. The Finite Element Method (FEM) results demonstrated a significant correlation with the experimental response, particularly in terms of the load-displacement curve failure mode. Once the model was validated, various alternative designs were numerically tested to evaluate the impact of each model on the load-bearing capacity. These designs included altering the height of the CFRP sheet, adjusting the height and congestion of the CFRP bar, and comparing the performance of the concrete jacket with and without the CFRP sheet. After reinforcing the CFRP sheets and incorporating Near-Surface-Mounted (NSM)-CFRP bars, the reinforcement system, along with the new concrete jacket, effectively transferred the integrity of the broken pier area and maintained a constant load-bearing capacity for the bridge pier. However, when the CFRP sheet was added to the aforementioned system, the load capacity of the bridge pier increased by more than 60%. Therefore, it can be concluded that seismic enhancement techniques utilizing CFRP sheets and mounted NSM-CFRP bars are successful in enhancing the strength and resilience of the concrete bridge pier. (DOI:**https//doi.org/10.52547/JCER.5.4.1**)

Keywords: Near-surface-mounted (NSM), Carbon Fiber Reinforced Polymer (CFRP), Numerical model, Seismic Strengthening

1. Introduction

An earthquake, a destructive natural phenomenon, has occurred in many regions around the world. There has been an increase in the frequency of earthquakes in recent times, leading to significant damage to bridges. Past experiences have taught us that the bridge piers are particularly vulnerable during earthquakes [1]. To enhance the seismic resistance of bridges, retrofitting methods have been developed, focusing on covering or coating the bridge piers with

* Corresponding author. Tel.: +989125148269; e-mail: bakhtiariamir96@gmail.com.

various materials such as steel pipes, thin concrete layers, carbon fiber reinforced polymer (CFRP), and other advanced composites [2]. Fiber-reinforced polymer (FRP) composites are an incredibly versatile technology that has proven to be highly efficient and advantageous. They possess a strong strength-to-weight ratio, do not corrode, require less labor, can be deployed quickly, and have lower long-term maintenance costs. FRP products find applications both for internal and external reinforcement of structures [3]. Different forms of FRP components like boards, laminates, rigid structures, bars, and tendons are crucial for the structural integrity of bridges. State-of-the-art articles provide detailed information on various aspects of FRP implementation, including reliability, statistical features, research methodology, and long-term performance. Recent studies have focused on the effectiveness of near-surface-mounted (NSM) FRP laminates to strengthen existing reinforced concrete (RC) beams [4], [5].

The NSM technique typically employs reinforcement that is produced via a pultrusion process, similar to the FRP rebars. These reinforcements may have a cross-section that is either round or square in shape. To achieve structural integrity, the reinforcement bars are carefully placed in grooves that are cut into the underside of the beam [6]. The adhesive utilized for bonding purposes is a high-viscosity epoxy or a cement paste [7]. By incorporating FRP rods into these grooves, the use of NSM reinforcement can substantially enhance the Flexi-security of RC beams, as well as improve their overall efficiency [8]. In particular, the NSM technique effectively shifts the failure zone from the column to the beam, thereby offering supplementary strength or ductility [9], [10]

The primary benefit of employing the NSM pre-stress strategy is its ability to enhance serviceability by effectively controlling flexural cracks, mitigating service load defects, and prolonging the initiation of steel reinforcement [8]. Extensive research has been conducted on the use of NSM FRP reinforcement to reinforce concrete beams, primarily focusing on concrete slabs [11], [12]. However, limited studies have been performed on the application of NSM FRP in bolstering columns. This is mainly due to the prevailing belief that NSM FRP laminates are ineffective in compression, as highlighted by Fib Bulletin 14 [13], which states that the compression elasticity modulus of FRP is lower than its stress module. This perception has hindered the widespread utilization of NSM FRP laminates for enhancing the strength of concrete columns [14], [15]. These findings are in line with the guidelines put forth by ACI 440.2R [16]

According to reports, it is not recommended to utilize FRP systems as a means to enhance compressive strength. The CAN/CSA S806 standards [17] have clarified that the reinforcement elements of FRP used in the compression zone of concrete are deemed to possess negligible compressive strength and rigidity with regard to construction purposes. ACI 440.2R does not endorse the utilization of FRPs for compression [16]

In view of the potential occurrence of premature defects [18], [19], such as the buckling of fibers on a small scale, unsupported or poorly preserved laminates buckling, and insufficient anchoring of substrates and FRP surfaces, alongside the unreliability of the compressive strength of laminates, it is crucial to address these issues [20], [21]. The micro buckling problem may arise from inadequate quality control of the FRP production, which might be attributed to the presence of ACI 440.2R vacuum in the resin [22]. However, adhering to quality control measures can effectively solve this problem.

As part of our study, we have examined the utilization of high-module externally bonded longitudinal FRPs on slender reinforced concrete (RC) columns. Our findings indicate that incorporating longitudinal FRP laminates enhances the load-carrying path of slender columns and optimizes their axial performance [23], [24]. This improvement is achieved by fortifying the stiffness of the columns through additional reinforcement provided by the longitudinal FRP laminates [25], [26].

In relation to the absence of compression laminates FRP and their effectiveness in terms of compressive behavior, it is crucial to thoroughly examine the compression behavior of NSM FRPs. Insufficient research has been conducted on the suitability of longitudinal compressive NSM FRP laminates in both bending and axially loaded cement bridge columns, particularly in terms of their strength, rigidity, and understanding of compression characteristics of FRPs. The potential risks associated with premature

cracking, corrosion, and buckling failure in NSM FRP reinforced concrete columns highlight the necessity for further studies. A model is utilized to determine the optimal design parameters for the specimens at a later stage. The primary objective of this research is to investigate the performance of the bridge column. It aims to design a hybrid solution that can maximize the benefits of CFRP while mitigating its drawbacks. The numerical analysis includes enhancements to the concrete and CFRP dimensions, the length and width of the CFRP layer, and modifications to the NSM bar dimensions. The bridge specimens are classified into eight distinct categories and simulated using a finite element method program. These specimens undergo monotonic loading tests in order to identify the most effective reinforcement schemes for new structures.

2. Experimental tests

The experimental investigation was carried out by Chen [27] has been used to validate numerical modeling. In this study, a scale model pier was designed, based on a 1/8 scale prototype pier [27]. The test setup and the retrofitting scheme are shown in Fig. 1(a). The height of the pier model was 2,500 mm and the cross section was 640×450 mm. In this case, the CFRP jacket was used on the pier faces in such a manner that one layer of the CFRP sheet is used in the longitudinal and transverse directions, the longitudinal layer is first wrapped and the transverse layer is then coated [27]. In addition, a new 20 cm high concrete jacket is constructed over the anchored reinforcement and forms an extended reinforced concrete frame to preserve the bottom-anchoring impact that the binding specimen is positioned at the end of the pier. The concrete used for the attachment had a compression power of 28 days of 30 MPa. Also, the steel used in both the longitudinal bars and the stirrups had an elasticity modulus of 210 GPa, the Poisson ratio was 0.3, the Yield tension of the stirrups was 335 MPa and the yield pressure of the longitudinal reinforcements was 335 MPa. The CFRP used for retrofitting had an elastic modulus of 243 GPa and a Poisson ratio of 0.3. The description of the specimen and the CFRP arrangement used is seen in Fig.1(b) [27].

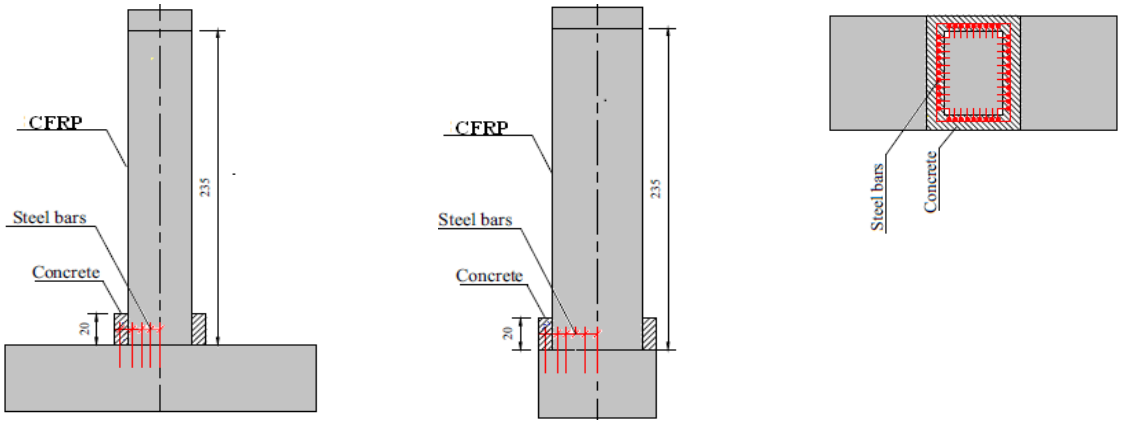

(a)

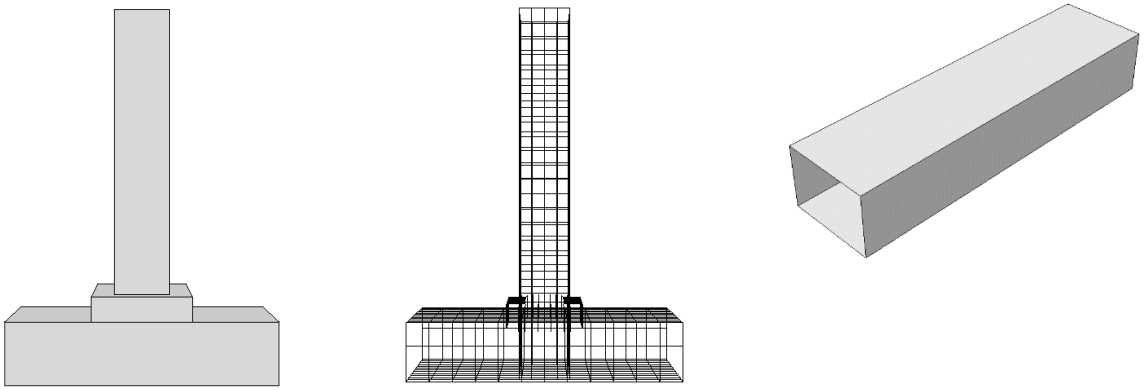

(b)

Fig. 1 View of the rebar and concrete arrangement [27].

3. Finite element method (Numerical models' description)

ABAQUS [28] General intent of the finite element program was used to model laboratory experiments to include a general technique that was commonly applicable to clinicians. The following subsections deal with geometry, components, mesh, boundary conditions, contacts, and estimation process descriptions of the model is applied. Models were divided into 3D sections, one for CFRP sheets, one for GFRP bars, one for concrete, and one for bars. With mesh and without mesh models, the experimental models developed in the laboratory and the corresponding measurements are shown in Fig. 3.

Fig. 3. displays the models (A to G) which were numerical models created by simulator software and the corresponding dimensions.

3.1. Materials in FEM

Concrete Damage Plasticity (CDP) was used in the composite pier simulation to describe the concrete behavior of FE modeling. The CDP model was built based on two concrete failure mechanisms: compressive crushing and tensile cracking [29],[30]. It combines isotropic, weakened elasticity with compressive plasticity and isotropic tensile. The two major failure mechanisms are called tensile cracking and compressive crushing of concrete [31],[32],[33]. After trying a lot of values, the following values selected as the most suitable ones; 0.15 for the Poisson's ratio of concrete, 30 degrees for the dilation angle Ψ of the reinforced concrete, and [34],[35] for nonlinear uniaxial behavior of concrete, the Kent and Park formulation was used [36]. According to this, compressive stress is calculated by equation (1):

$$\sigma_C = f'_{co}\left[2\left(\frac{\varepsilon_c}{\varepsilon'_c}\right) - \left(\frac{\varepsilon_c}{\varepsilon'_c}\right)^2\right] \quad (1)$$

Where ε_c is the compressive strain, f'_{co} and ε'_c are the compressive strength of unconfined cylindrical concrete specimen and the related strain respectively. The value of ε'_c is considered to be 0.002.

The compression damage parameter (dc), controls the unloading gradient of the stress-strain curve. In concrete and similar materials, such as masonry materials, the higher the plastic strain, the slope of the unloading curve will be reduced to a greater extent than the initial gradient (elasticity specimen). It is due to the damage caused by the loss induced in a brittle material. When damage starts, compressive stress is calculated based on the following equations (2) and (3) [31],[37],[38]:

$$\sigma_C = (1 - d_c)\, E_O\, (\varepsilon_C - \varepsilon_C{}^{\sim PL} \quad (2)$$

$$\varepsilon_C{}^{\sim PL} = \left(\varepsilon_C{}^{\sim in} - \frac{1}{(1 - d_{c)}}\frac{\sigma_c}{E_0}\right) \quad (3)$$

Where $\varepsilon_C{}^{\sim PL}$ is an inelastic strain, ε_C is the compressive strain, E_O is elasticity modulus, d_c is compressive damage, $\varepsilon_C{}^{\sim in}$ is strain related to damage.

Finally, equation 4 is used to calculate the compressive damage value dc [28]:

$$dc = 1 - \frac{\sigma_c}{f'_{co}} \quad (4)$$

For the simulation of the internal CFRP bar, two linear 3D truss elements (T3D2) were used to discrete the concrete volume, while three nodes triangular general-purpose shell finite membrane strains (S3R) were used with CFRP. Two node 3D truss elements were also used in the simulation of the internal CFRP bar [33],[36],[39]. Various grids according to each part's thickness (concrete, CFRP bar, and CFRP sheet) were applied. The convergence of digital solutions was controlled with mesh measurements of 100, 75, 50, and 25 mm in the concrete region and the mesh size of 50 mm was selected. It has been believed that the interaction between CFRP and the concrete is perfectly connected (tie). An integrated relationship of the CFRP bar with the concrete was modeled [40]. The Pier model was simply supported at the corresponding span and the load was indirectly modeled as an imposed displacement on the pier top. The reaction force associated with this imposed displacement was taken as the applied force. The procedure of analysis was done in implicit mode. Regarding quasi-static loading, the static general step was selected for analysis. For running 1 model, the Calculation time was approximately 23 hours with Intel® core i7 CPU.

3.2. Model fitting

In the key representative situations, experimental testing of CFRP bridge pier was selected to match the numerical model: with an attached carbon fiber plate. The default Kc = 0.667 values deliver the most reliable results of ultimate power and failure. The dilation angle (Ψ) ranged from 25 to 35 and the viscosity parameter for concrete harm measurements had a value of 0,001. Higher dilation angle values produce ductile response while lower dilation angle values give a fragile response. Compression (dc) measured damage parameter has a remarkable effect on the bending response of the hybrid structural elements. The use of a larger parameter for viscosity will reduce the measuring time considerably, but the results are worse. The conclusion shows that the value of the viscosity parameter must be carefully chosen and measured accordingly in realistic calculations using the CDP material model. The dilation, Kc, and viscosity values equal to 30, 1.16, and 0.667, respectively, are taken for the best fit. These values are consistent with Abaqus's guidance on the damaged plasticity of concrete and other research results [31]. According to CEB-FIB, the concrete stress-strain compression and the tensile post cracking behavior of the concrete were defined [39]. The results for the best fitting parameters are reported is shown in Fig 2. Between the experimental and numerical curves, a strong agreement can be seen. In particular, maximum loads were predicted with an average relative error of 3% (114.52kN predicted vs. 116.44kN experimental for the cases). The numerical model tends to slightly underestimate experimental load-bearing capacity. Regarding the stiffness, the model accurately predicts the force-displacement slope in most of the force increase range. As long as the CFRP-concrete contact was supposed to be completely bonded, when this condition is lost the model convergence is no longer possible and there is no predicted data for the post-critic response. Nevertheless, the loading branch is the most significant for designing procedures which was the initial aim of the research.

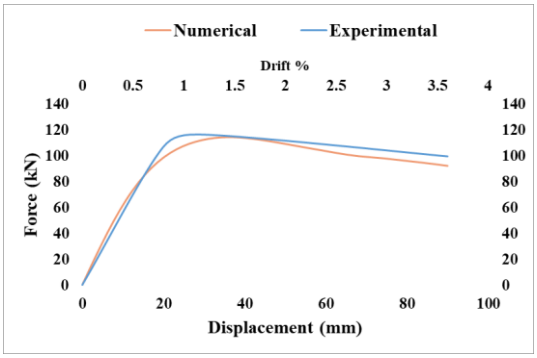

Fig. 2. The experimental and numerical load-deflection curves of the specimen bridge pier with CFRP

4. Geometric parameters study

To evaluate the performance of bridge pier configuration, various geometries were simulated with the parameters fixed in the previous fitting process. Simulated cases are summarized in Fig. 3.

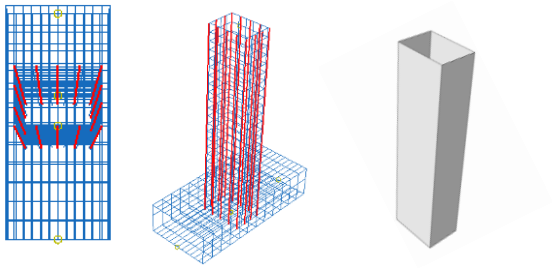

1) Case A. Concrete 2500 mm in height, section 640 × 450 mm. The pier sides were used in the CFRP jacket 2500 mm CFRP process, NSM CFRP bar so that, longitudinal direction in 5, transverse direction in 4, 20 mm width, 2500 mm height and 6 mm longitudinal diameter.

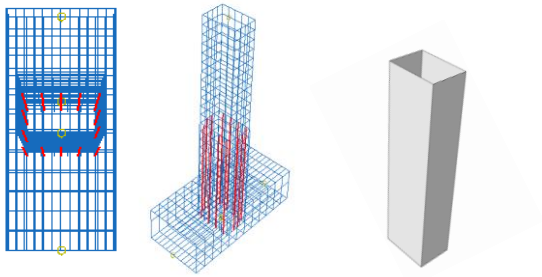

2) Case B. Concrete 2500 mm in height, section 640 × 450 mm. 2500 mm CFRP jacket, method NSM, CFRP bar were used in the pier faces Such that in the longitudinal direction in 5, in the transverse direction in 4 mm, in the depth of 20 mm, in the height of 1480 mm and the diameter of the longitudinal bar 6 mm.

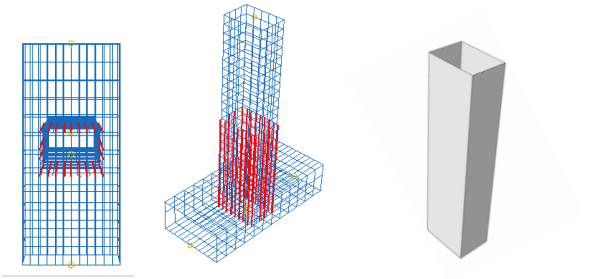

3) Case C. Concrete 2500 mm in height, section 640 × 450 mm. 2500 mm CFRP jacket, method NSM, CFRP bar is used in pier faces Such that the longitudinal direction is 9, the transverse direction in 4 mm, the depth of 20 mm, the height of 1480 mm and the diameter of the longitudinal bar in 6 mm.

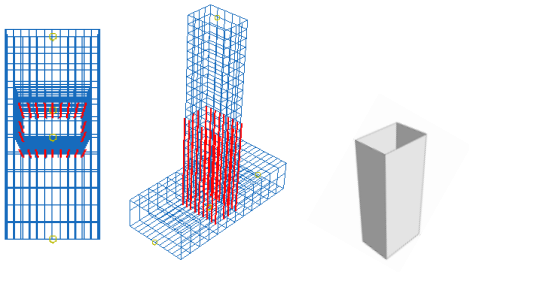

4) Case D. Concrete 2500 mm in height, section 640 × 450 mm. 1500 mm CFRP jacket, method NSM, CFRP bar were used in the pier faces In such a way, the longitudinal direction is 9, the transverse direction in 4 mm, the depth of 20 mm, the height of 1480 mm and the diameter of the longitudinal bar 6 mm.

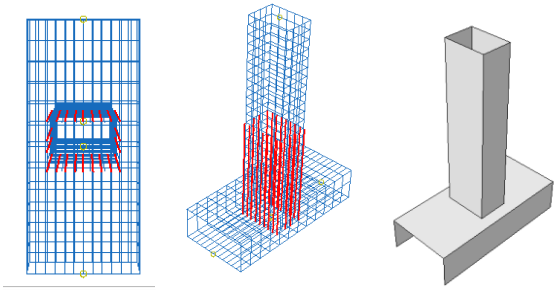

5) Case E. Concrete 2500 mm in height, section 640 × 450 mm. 1500 mm CFRP jacket and the base is also reinforced with a CFRP jacket, the NSM process, the CFRP bar has been used in the pier faces Such that the longitudinal direction is 9, the transverse direction in 4 mm, the depth of 20 mm, the height of 1480 mm and the diameter of the longitudinal bar is 6 mm.

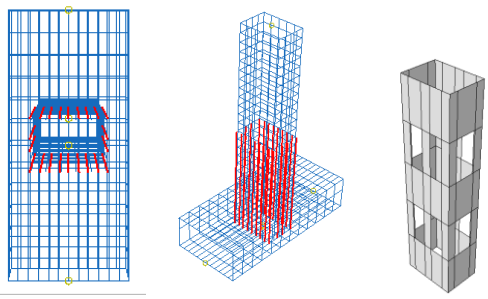

6) Case F. Concrete 2500 mm in height, section 640 × 450 mm. But the CFRP sheet was reduced by 30%, the NSM process, the CFRP bar is used in the pier faces So that the longitudinal direction is 9, the transverse direction in 4 mm, the depth of 20 mm, the height of 1480 mm, and the diameter of the longitudinal bar in 6 mm.

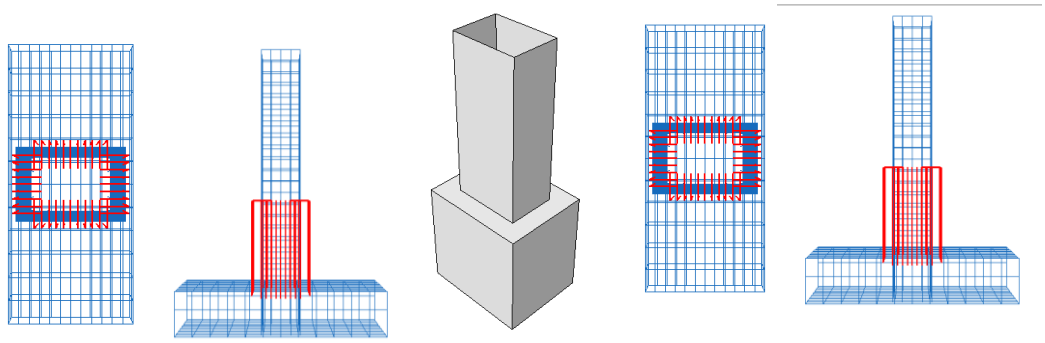

7) Case G. The model pier had a height of 2500 mm and its scale was 640 × 450 mm. CFRP jackets were used in the pier faces in such a way that one layer of CFRP sheet is used in the longitudinal and transverse directions, respectively. Besides, a new concrete jacket, 100 cm thick, is placed around the anchored reinforcement.

8) Case H. The height of the model pier was 2500 mm and the cross-section was 640 × 450 mm. There is no CFRP jacket in this specimen. Besides, a new concrete jacket, 100 cm thick, is placed over the anchored reinforcement. 20 mm deep, 1480 mm high, and 6 mm longitudinal bar diameter.

Fig. 3. Bridge pier, the cases under consideration.

5. Analysis of the force-displacement curves

In Fig. 4, force-displacement curves of cases A, B, C, D, E, F, G, and H are compared with those representing experimental tested cases. In Table 1, the values of ultimate strength (Fp), Deformation at the maximum capacity (du), and the area beneath the force-displacement curve (dissipated energy-Gd) are introduced. Results showed that increasing the concrete cross-section significantly increased the load-bearing capacity. Cases A and B, showed similar capacities, so increasing the height of the CFRP bar (NSM) is no effect if the CFRP-concrete jacket connection is assured. In case C, the intensity of the CFRP rebar (NSM) at the intersection between the column and the foundation causing a reduction in the system's dissipated energy in comparison with cases A, although the maximum load-bearing capacity was maintained. Comparing case D with cases A and B, the reduction in the height of the CFRP jacket was expected to reduce dissipated energy and maximum load-bearing capacity. Comparison of case E with case C shows that the retrofit of the foundation with the CFRP jacket does not affect increasing dissipated energy and maximum load-bearing capacity. Comparison of case F with case C shows that the use of the CFRP window arrangement has increased the increasing dissipated energy and maximum load-bearing capacity due to the reduced interaction between concrete and CFRP. Cases G and H had greater concrete area so showed greater initial stiffness although, the use of CFRP in Case G has increased increasing dissipated energy and maximum load-bearing capacity.

5.1. Analysis of the maximum plastic strain index

The ultimate plastic strain (Pe) criterion is an appropriate parameter in estimating the damage in concrete. This is a suitable criterion for investigating the number of cracks and the tensile and compression failures along with their alignment. Concrete damage is related to the CFRP-concrete debonding process. Tensile Damage Parameters (DAMAGET), compression damage (DAMAGEC), and stiffness Determination (SDEG) are other parameters that can be used to assess damage in concrete structures [32],[41]. Although these particular parameters are useful for evaluating the amount of damaged concrete, PE is more commonly used [31].

The model for the experimental case with mesh reached a maximum plastic strain value of about 0.454%, which indicated extensive tensile damage in concrete, and most of the cracks were formed at the intersection between the column and the foundation. The greatest cracks in this area were expected and obtained by the model as can be seen in Fig. 5 and Table 2.

The overall key plastic pressure is elevated as a function of the strength of the CFRP Rebar (NSM) and the wider concrete region showing the stress accumulation and a related rise in injury.

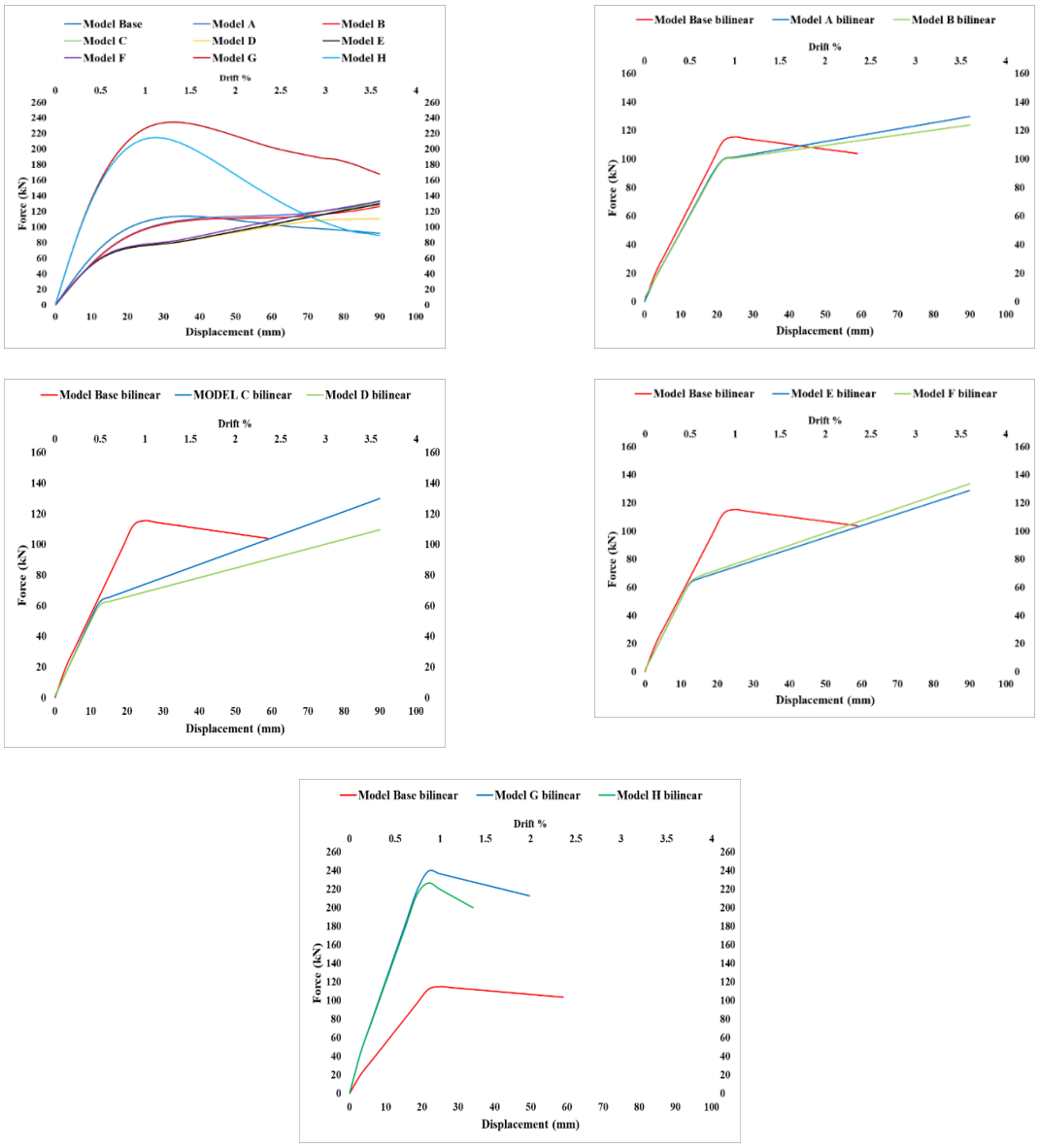

Fig. 4. Comparison of Force-Displacement curves for cases

Table 1.

Ductility ratio and the related factors in retrofitted and base cases

Cases	dy (mm)	du (mm)	$\mu = \frac{d_u}{d_y}$
Base	21.72 (0.87)	58.96 (2.36)	2.71
A	21.72 (0.87)	90 (3.6)	4.15
B	21.72 (0.87)	90 (3.6)	4.15
C	12.41 (0.50)	90 (3.6)	7.25
D	12.41 (0.50)	90 (3.6)	7.25
E	12.41 (0.50)	90 (3.6)	7.25
F	12.41 (0.50)	90 (3.6)	7.25
G	18.62 (0.75)	49.65 (1.98)	2.67
H	18.62 (0.75)	34.14 (1.37)	1.84

Table 2.

The maximum load-carrying capacity, the dissipated energy, and maximum principle plastic stain for all the cases

Cases	Maximum strength (kN)	Deformation at the maximum capacity (mm)	dissipated energy (kN.mm)	Maximum principal plastic strain (%)
Base	115.53	24.82	5375	0.454
A	130.15	90	9008	0.289
B	124.08	90	8780	0.267
C	130.17	90	7912	0.436
D	109.71	90	7025	0.424
E	128.95	90	7886	0.431
F	133.82	90	8115	0.464
G	239.62	21.72	9153	0.811
H	226.66	21.72	5405	0.690

In the case of A, the tensile damage to concrete (PE0.289 %) was seen to reduce as the height of the CFRP sheet increased. On the other hand, the case B with the decreased height of the CFRP bar (at the intersection between the column and the foundation region) showed that the tensile damage in concrete (PE0.267 %) was decreased when the height of the CFRP was reduced. When increasing the congestion bar between NSM (CFRP bar) in concrete (case C) there was less concrete at the intersection between the column and the foundation region of the case and the CFRP bar was concentrated there Increasing the possible tensile damage in concrete to PE=0.436% but reaching similar load-bearing capacity to the experimental case A. Increased concrete cross-section (case G and H) will significantly increase the system's shear capacity and eliminate the cracks at the crossroads between the column and the foundation area. In the case of G due to the use of FRP, PE achieved the highest value among the models: 0.811 trillion. This reality suggests that this case was the one that enabled the creation of more tensile damage in concrete, while higher loads were supposed to be resisted. A representative contour plot of the PE index is provided in Fig.5.

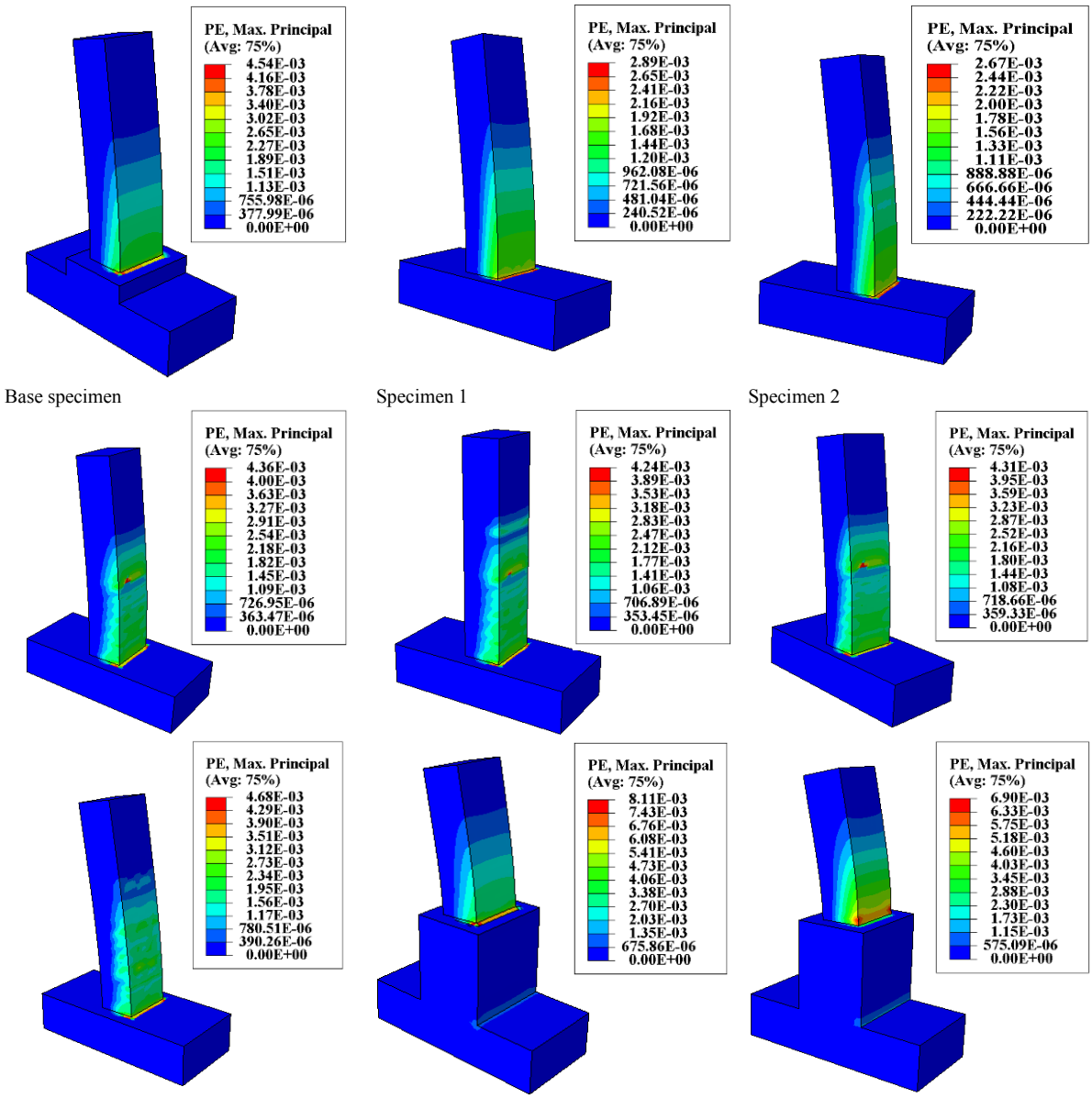

Fig. 5. Maximum principal plastic strain in the base and the proposed cases.

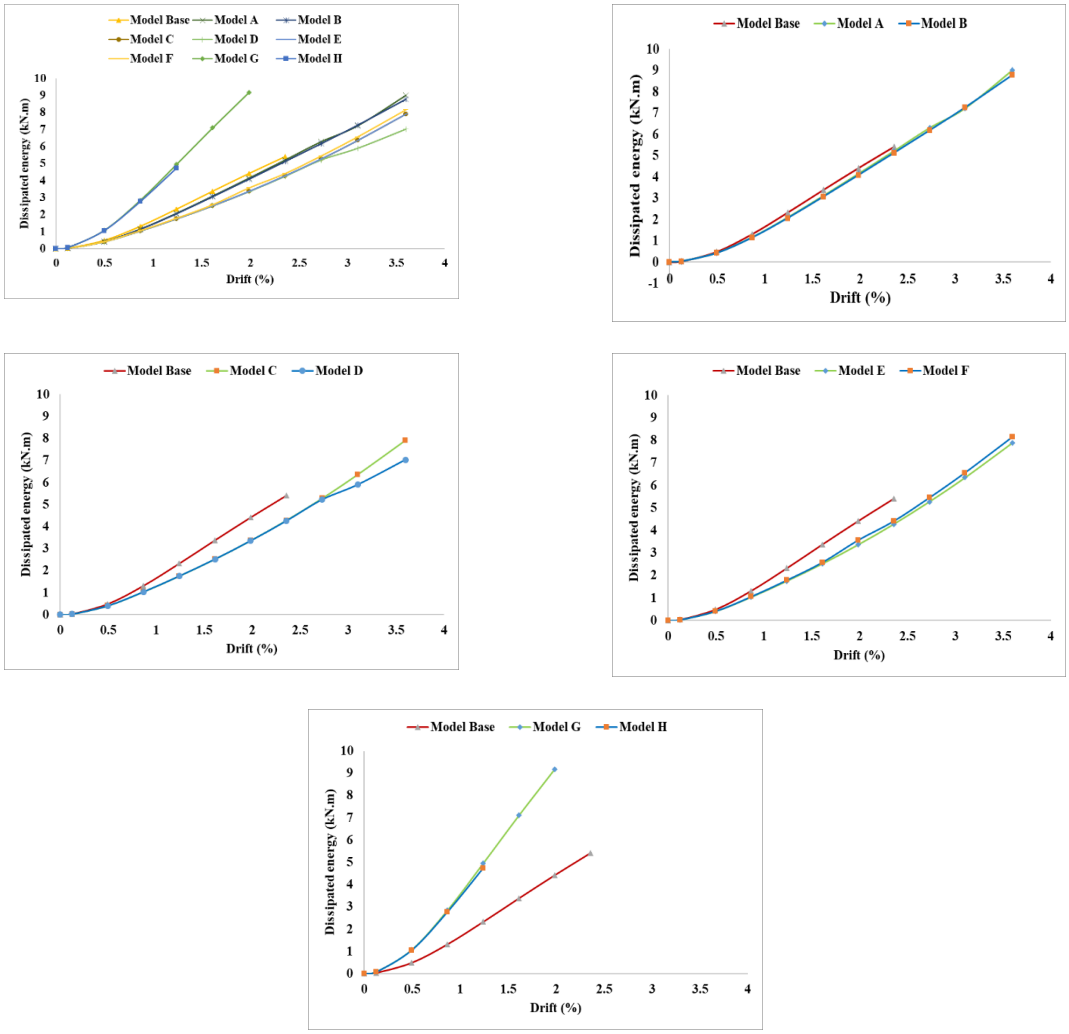

Fig. 6. Evolution of the dissipated energy during the monotonic loading in the base and the proposed specimens

5.2. Dissipated energy

The energy dissipation and inelastic deformation of the elongation load resistance system signify the ability of the structure to withstand the loading requirements of the seismic event. At each loading point, the sum of dissipated energy could be determined from the enclosed area as shown by the monotonous reaction of the lateral load vs. the lateral displacement. The addition of dissipated energy associated with the increase in lateral elongation would result in total dissipated energy at each point of inter-story elongation. The evolution of dissipated energy for all specimen states was shown in Fig. 6. Dissipated energy is analyzed in three areas of 1, 2, and 3, with area 1 being 0 to 1 drift and area 2 being 1 to 2.5 drifting, and area 2 being 3 being 2.5 to 3.5 drifting distances. Both specimens were related to the base specimen. Cases A, B, C, and D gave an energy dissipation potential of less than one base specimen in the respective specimen in areas 1 and 2 of the loading processes. Cases G and H have given an energy dissipation potential comparable to the base in all areas (1,2 and 3).

5.3. Analysis of secant stiffness

As a result of reversing and repetitive acts of monotonic loading, the stiffness of the Concrete Bridge Pier structure will deteriorate. Similarly, stiffness is often decreased along with an increase in load after plasticization effects have occurred. Secant stiffness related techniques use secant stiffness at the design reaction stage and the principle of equal viscous damping to describe the nonlinear behavior of structural structures [42]. Fig. 7. It also demonstrates how the secant or effective stiffness, K_{eff}, is defined as the strength ratio, VB, to the maximum possible displacement. In all modeled cases, the secant stiffness is assumed to be the slope of the straight line which connects the peak loads to the positive displacement of the load versus the displacement enveloping at each stage of deformation. To determine this stiffness loss, the secant stiffness is measured at various loading stages during the simulated monotonic load rise. Relationships are seen in Fig. 8. The simulated cases in the following plots have been compared with the mesh experimental plots. The simulation of the experimental case base revealed a poor qualitative response to stiffness. Although CFRP had a higher modulus than concrete, its area and height increase did not compensate for the reduction of the stiffness response from case D to case E. This difference is reduced as tensile damage in concrete progress being no appreciated for the highest loads. Declining the separation between the concrete of the CFRP sheet (case D and F compared with case A) reduced the stiffness of the system although differences tended to decrease as load increased and the tensile damage progress. Removing a significant part of the bottom CFRP (case E) was associated with the lowest stiffness all simulated test long. Cases G and H showed greater stiffness than the experimental case. Both had greater concrete area than the comparison case, being more effective.

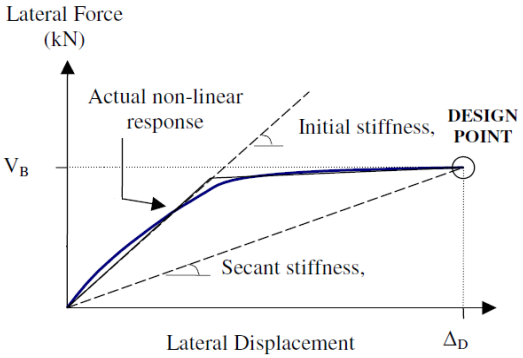

Fig. 7 Usage of initial-stiffness and secant stiffness concepts related to the complete non-linear response of the structure and its equation [42].

6. Conclusions

In this research, a comprehensive numerical analysis was performed to investigate the seismic strengthening of the concrete bridge pier, Hybrid systems, such as the carbon fiber-reinforced polymer (CFRP) sheet attached to the concrete, the Near-Surface-Mounted (NSM)-CFRP bar, and the Concrete jacket. Nine Concrete bridge pier systems with various geometries were simulated assuming concrete damaged plasticity (CDP). One of them was used to fit model parameters with experimental available results

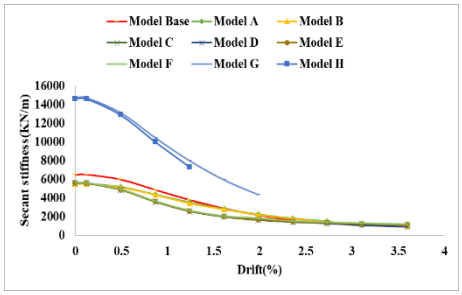

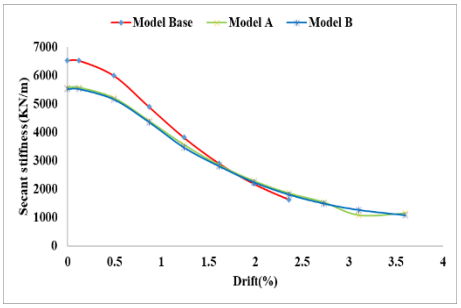

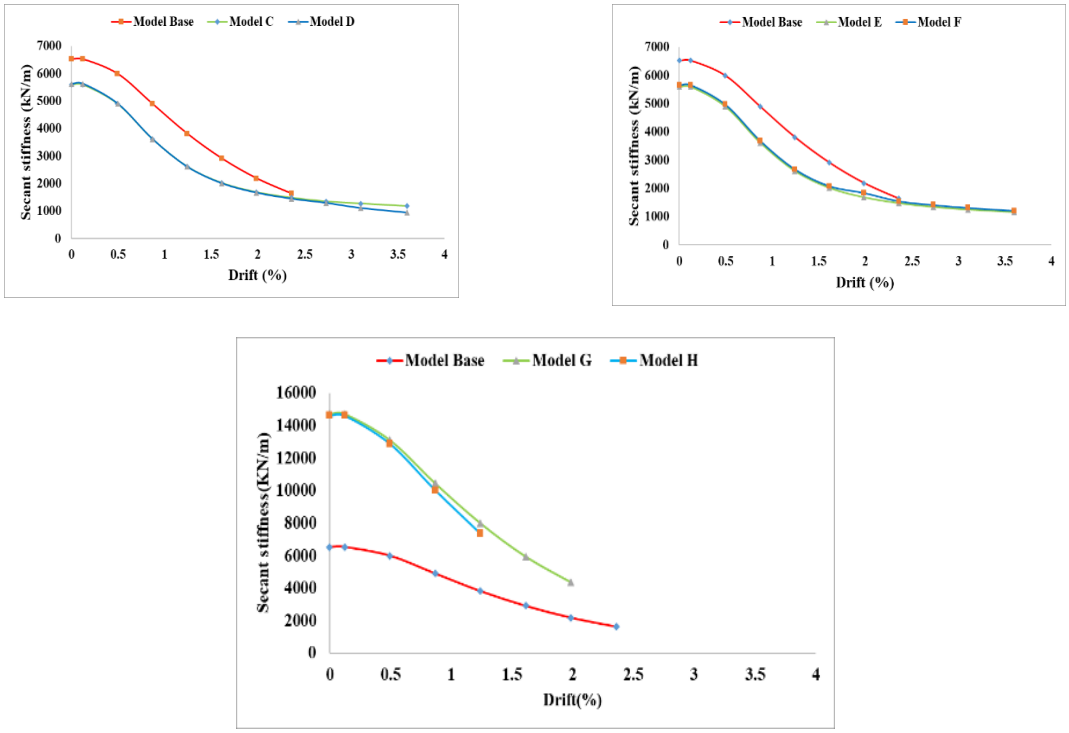

Fig. 8. Secant stiffness evolution

and the other seven to analyze possible alternative design options. From the pieces of evidence, it is possible to conclude:

1. The recommended model fitted full experimental force-displacement curves with a slight underestimation of the maximum load-bearing capacity of less than 3%.

2. Concrete damage plasticity dilation angle and viscosity are the most sensitive parameters to be adjusted in the model.

3. Increasing the width of concrete did not provide greater load-bearing capacity per unit width but a slightly stiffer response because of the higher proportion of concrete in the section.

4. Results showed that increasing the concrete cross-section significantly increased the load-bearing capacity. Cases A and B, showed similar capacities, so increasing the height of the CFRP bar (NSM) is no effect if the CFRP-concrete jacket connection is assured

5. The retrofitting techniques using a CFRP sheet and NSM-CFRP bar demonstrated that the strength and capability of the concrete bridge pier could be significantly improved, especially to strengthen the strength. The lateral carriage capability of the bridge pier increased by over 60% after reinforcement. Some problems remain, such as how the cost-efficient use of reinforcing materials in real structures to achieve a satisfactory outcome are needed for further study.

References

[1] O. Hassanshahi, T. A. Majid, T. L. Lau, A. Yousefi, and R. M. K. Tahara, “Seismic performance of the typical RC beam–column joint subjected to repeated earthquakes,” 2017, p. 120014. doi: 10.1063/1.5005755.

[2] C. L. Oh, K. K. Choong, T. Nishimura, J.-Y. Kim, and O. Hassanshahi, “Shape change analysis of tensegrity models,” Latin American Journal of Solids and Structures, vol. 16, no. 7, 2019, doi: 10.1590/1679-78255407.

[3] A. Mahboob, L. Gil, E. Bernat-Maso, and A. R. Eskenati, “Experimental and Numerical Study of Shear Interface Response of Hybrid Thin CFRP–Concrete Slabs,” Materials, vol. 14, no. 18, p. 5184, Sep. 2021, doi: 10.3390/ma14185184.

[4] A. Mahboob, L. Gil, E. Bernat-Maso, and A. R. Eskenati, “Flexible Fiber Fabric for FRP–Concrete Connection of Thin

Hybrid Slabs," Polymers (Basel), vol. 13, no. 17, p. 2862, Aug. 2021, doi: 10.3390/polym13172862.
[5] A. Salles, M. Salati, and L. Bragança, "Analyzing the Feasibility of Integrating Urban Sustainability Assessment Indicators with City Information Modelling (CIM)," Applied System Innovation, vol. 6, no. 2, p. 45, Mar. 2023, doi: 10.3390/asi6020045.
[6] G. M. Dalfré and J. A. O. Barros, "NSM technique to increase the load carrying capacity of continuous RC slabs," Eng Struct, vol. 56, pp. 137–153, Nov. 2013, doi: 10.1016/j.engstruct.2013.04.021.
[7] S. Abbasi, A. Mahboob, H. Bakhtiari Zamani, M. R. Bilesan, E. Repo, and A. Hakimi, "The Tribological Behavior of Nanocrystalline TiO2 Coating Produced by Plasma Electrolytic Oxidation," J Nanomater, vol. 2022, pp. 1–13, Jan. 2022, doi: 10.1155/2022/5675038.
[8] H. Lee, W. T. Jung, and W. Chung, "Field test of an old RC bridge before and after NSM strengthening," Compos Struct, vol. 202, pp. 793–801, Oct. 2018, doi: 10.1016/j.compstruct.2018.04.024.
[9] A. Mahboob, O. Hassanshahi, and A. S. Tabrizi, "Three-dimensional simulation of granular materials by discrete element method (DEM) by considering the fracture effect of particles," Journal of Civil Engineering Researchers, vol. 5, no. 2, pp. 14–28, 2023.
[10] A. R. Eskenati, A. Mahboob, A. Alirezaie, R. Askari, and S. M. S. Kolbadi, "INVESTIGATING THE EFFECT OF LONGITUDINAL GALLERY ON DYNAMICAL RESPONSE OF GRAVITY CONCRETE DAMS USING FEM," Journal of Southwest Jiaotong University, vol. 56, no. 4, pp. 804–811, Aug. 2021, doi: 10.35741/issn.0258-2724.56.4.69.
[11] A. R. Eskenati, A. Mahboob, E. Bernat-Maso, and L. Gil, "Experimental and Numerical Study of Adhesively and Bolted Connections of Pultruded GFRP I-Shape Profiles," Polymers (Basel), vol. 14, no. 5, p. 894, Feb. 2022, doi: 10.3390/polym14050894.
[12] M. Salati, L. Bragança, and R. Mateus, "Sustainability Assessment on an Urban Scale: Context, Challenges, and Most Relevant Indicators," Applied System Innovation, vol. 5, no. 2, p. 41, Apr. 2022, doi: 10.3390/asi5020041.
[13] J. A. Bogas and A. Gomes, "Analysis of the CFRP flexural strengthening reinforcement approaches proposed in Fib bulletin 14," Constr Build Mater, vol. 22, no. 10, pp. 2130–2140, Oct. 2008, doi: 10.1016/j.conbuildmat.2007.07.025.
[14] W. Y. Peen, C. K. Keong, and O. Hassanshahi, "Behaviour of hollow circular section with multiple perforations under compression, flexure and torsion," Latin American Journal of Solids and Structures, vol. 16, no. 2, 2019, doi: 10.1590/1679-78255387.
[15] M. Abedi et al., "A self-sensing and self-heating planar braided composite for smart civil infrastructures reinforcement," Constr Build Mater, vol. 387, p. 131617, Jul. 2023, doi: 10.1016/j.conbuildmat.2023.131617.
[16] P. Silva and R. Kanitkar, "ACI 440.2 R and The New Seismic Strengthening Guidelines Using FRP," Special Publication, vol. 327, pp. 20–21, 2018.
[17] M. M. Hassan and A. Deifalla, "Evaluating the new CAN/CSA-S806-12 torsion provisions for concrete beams with FRP reinforcements," Mater Struct, vol. 49, no. 7, pp. 2715–2729, Jul. 2016, doi: 10.1617/s11527-015-0680-9.
[18] S. MOTAMEDPOOYA and E. ASNAASHARI, "Organizational project management maturity from the construction practitioners point of view," 2016.
[19] A. R. Eskenati, A. Mahboob, E. Bernat-Maso, and L. Gil, "Characterizing the Structural Behavior of FRP Profiles—FRCM Hybrid Superficial Elements: Experimental and Numerical Studies," Polymers (Basel), vol. 14, no. 6, p. 1076, Mar. 2022, doi: 10.3390/polym14061076.
[20] A. Mahboob, A. R. Eskenati, and S. Moradalizadeh, "Numerical Investigation and Cost Analysis of FRP-Concrete Unidirectional Hybrid Slabs," International Journal of Applied Mechanics and Engineering, vol. 26, no. 4, pp. 156–166, Dec. 2021, doi: 10.2478/ijame-2021-0056.
[21] A. Yousefi, N. M. Bunnori, M. Khavarian, O. Hassanshahi, and T. A. Majid, "Experimental investigation on effect of multi-walled carbon nanotubes concentration on flexural properties and microstructure of cement mortar composite," 2017, p. 020032. doi: 10.1063/1.5005663.
[22] N. Uddin, S. Cauthen, L. Ramos, and U. K. Vaidya, "Vacuum assisted resin transfer molding (VARTM) for external strengthening of structures," in Developments in Fiber-Reinforced Polymer (FRP) Composites for Civil Engineering, Elsevier, 2013, pp. 77–114. doi: 10.1533/9780857098955.1.77.
[23] M. Abedi et al., "A sustainable cementitious composite reinforced with natural fibers: An experimental and numerical study," Constr Build Mater, vol. 378, p. 131093, May 2023, doi: 10.1016/j.conbuildmat.2023.131093.
[24] A. Mahboob, O. Hassanshahi, A. Hakimi, and M. Safi, "Evaluating the Performance of Hollow Core Slabs (HCS)-Concrete and Simplifying Their Implementation," Recent Prog Mater, vol. 05, no. 02, pp. 1–15, Apr. 2023, doi: 10.21926/rpm.2302016.
[25] M. Abedi, O. Hassanshahi, J. A. O. Barros, A. Gomes Correia, and R. Fangueiro, "Three-dimensional braided composites as innovative smart structural reinforcements," Compos Struct, vol. 297, p. 115912, Oct. 2022, doi: 10.1016/j.compstruct.2022.115912.
[26] M. Golabchi and E. Asnaashari, "Identification of Iran's road construction project risks in order to implement sustainable development (Pavement Technologies and Construction Activities)".
[27] X. Chen, M. Ding, X. Zhang, Z. Liu, and H. Ma, "Experimental investigation on seismic retrofit of gravity railway bridge pier with CFRP and steel materials," Constr Build Mater, 2018, doi: 10.1016/j.conbuildmat.2018.06.102.
[28] Simulia, "Abaqus User's Manual version 2019," Dassault Systèmes Simulia Corp.: Providence, RI, USA. 2019.
[29] J. Lubliner, J. Oliver, S. Oller, and E. Oñate, "A plastic-damage model for concrete," Int J Solids Struct, 1989, doi: 10.1016/0020-7683(89)90050-4.

[30] J. Lee and G. L. Fenves, "Plastic-Damage Model for Cyclic Loading of Concrete Structures," J Eng Mech, 1998, doi: 10.1061/(asce)0733-9399(1998)124:8(892).
[31] H. Behnam, J. S. Kuang, and B. Samali, "Parametric finite element analysis of RC wide beam-column connections," Comput Struct, 2018, doi: 10.1016/j.compstruc.2018.04.004.
[32] I. A. Sharaky, M. Baena, C. Barris, H. E. M. Sallam, and L. Torres, "Effect of axial stiffness of NSM FRP reinforcement and concrete cover confinement on flexural behaviour of strengthened RC beams: Experimental and numerical study," Eng Struct, 2018, doi: 10.1016/j.engstruct.2018.07.062.
[33] Y. sumer, "Defining parameters for concrete damage plasticity model," Challenge Journal of Structural Mechanics, 2015, doi: 10.20528/cjsmec.2015.07.023.
[34] Z. Wu, X. Wang, X. Zhao, and M. Noori, "State-of-the-art review of FRP composites for major construction with high performance and longevity," International Journal of Sustainable Materials and Structural Systems, 2014, doi: 10.1504/ijsmss.2014.062757.
[35] D. Zhang, Q. Zhao, F. Li, and Y. Huang, "Experimental and numerical study of the torsional response of a modular hybrid FRP-aluminum triangular deck-truss beam," Eng Struct, 2017, doi: 10.1016/j.engstruct.2016.12.007.
[36] D. Kent and R. Park, "FLEXURAL MEMBERS WITH CONFINED CONCRETE," Journal of the Structural Division, 1971.
[37] A. Demir, N. Caglar, H. Ozturk, and Y. Sumer, "Nonlinear finite element study on the improvement of shear capacity in reinforced concrete T-Section beams by an alternative diagonal shear reinforcement," Eng Struct, 2016, doi: 10.1016/j.engstruct.2016.04.029.
[38] A. Ganganagoudar, T. G. Mondal, and S. Suriya Prakash, "Analytical and finite element studies on behavior of FRP strengthened RC beams under torsion," Compos Struct, 2016, doi: 10.1016/j.compstruct.2016.07.014.
[39] I. Vilanova, L. Torres, M. Baena, and M. Llorens, "Numerical simulation of bond-slip interface and tension stiffening in GFRP RC tensile elements," Compos Struct, 2016, doi: 10.1016/j.compstruct.2016.06.048.
[40] M. H. Seleem, I. A. Sharaky, and H. E. M. Sallam, "Flexural behavior of steel beams strengthened by carbon fiber reinforced polymer plates - Three dimensional finite element simulation," Mater Des, 2010, doi: 10.1016/j.matdes.2009.09.010.
[41] V. V. Degtyarev, "Concentrated load distribution in corrugated steel decks: A parametric finite element study," Eng Struct, 2020, doi: 10.1016/j.engstruct.2019.110158.
[42] T. J. Sullivan, G. M. Calvi, and M. J. N. Priestley, "Initial Stiffness Versus Secant Stiffness in Displacement Based Design," 13th World Conference on Earthquake Engineering, 2004.